CARBON 48 (2010) 2677–2689

available at www.sciencedirect.com

journal homepage: www.elsevier.com/locate/carbon

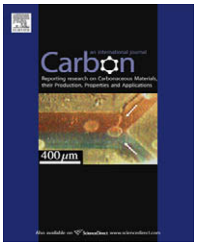

Review

Nanopatterning of graphene with crystallographic orientation control

László P. Biró [a,*], *Philippe Lambin* [b]

[a] *Research Institute for Technical Physics and Materials Science, H-1525 Budapest, P.O. Box 49, Hungary*
[b] *Facultés Universitaires Notre-Dame de la Paix, B-5000, Namur, Rue de Bruxelles 61, Belgium*

ARTICLE INFO

Article history:
Received 30 October 2009
Accepted 11 April 2010
Available online 14 April 2010

ABSTRACT

The recent papers on the nanopatterning of graphene and cutting of graphene nanoribbons were reviewed. It was found that until now the simultaneous control of crystallographic orientation and of the ribbon width in the range of nanometers was possible only by scanning tunneling lithography. The cutting process by local anodic oxidation under the AFM tip is a similar process, but due to the different physical interaction mechanisms of the STM and AFM tip with the substrate, and due to the larger radius of the AFM tip, the resolution of AFM lithography is poorer. The various cutting processes based on mobile, catalytic nanoparticles yield trenches with well defined crystallographic orientation, but have a major drawback: the location of the nanoparticles and the control of the direction in which the cutting will start are currently not predictable. The first promising results of a solid phase reduction reaction of the SiO_2 substrate at the graphene edge indicate the possibility of developing a new type of lithography that will allow the realization of complex nanopatterns. Recent results pointing to the possibility of the engineered modification of graphene edges may prove useful to all lithographic processes.

Contents

---

[*] *Corresponding author:* Fax: +36 1 392226.
E-mail address: biro@mfa.kfki.hu (L.P. Biró).
URL: http://www.nanotechology.hu/.

0008-6223/$ - see front matter
doi:10.1016/j.carbon.2010.04.013

1. Introduction

Its exciting properties [1] brought graphene very quickly in the focus of the attention of many research groups working in the field of nanocarbons. The success story of this single atom thick allotrope of carbon was started after a simple and very ingenious method [2] was proposed by Novoselov et al. to prepare this material that “should not exist” [1]. The possibility of ever manufacturing this material in a controlled way as a free standing sheet seemed unlikely for a long time as 2D crystals were thought to be thermodynamically unstable [3,4]. “Graphene” as a scientific terminology designating a one single atom layer thick graphitic sheet has entered the International Union of Pure and Applied Chemistry (IUPAC) nomenclature in 1994 in the context of graphite intercalation compounds [5]. The denomination was proposed in 1986 by Boehm et al. [6]. Interestingly enough, several years before the experimental success of Novoselov et al., the possibility of purposefully producing graphene layers was mentioned in a paper by Lu et al. [7]. A recent review of the field of graphene production enumerates several companies ready to produce tons of graphene [8]. Most of this material is produced by one of many variations on the general method of chemical exfoliation [9–14], including using organic solvents to enhance exfoliation [15,16]. Unfortunately even after hydrazine reduction of graphite oxide some detrimental effects on the electronic properties may persist [14,17]. Thus for nanoelectronic applications the best quality samples are produced by mechanical exfoliation [2]. Various CVD and epitaxial processes are also explored to produce high quality graphene. Graphene epitaxy on SiC is a well established method [18,19], unfortunately the first graphene layer interacts strongly with the substrate [19,20]. CVD growth of graphene on Ni [21] or Ni thin films [22] is also a promising way of producing large area, high quality sheets. Other metals like Ru [23] and Cu [24] have also been used as substrates, even highly oriented pyrolytic graphite (HOPG) has been used for graphene epitaxy [25]. Whichever substrate and growth method is used, if nanoelectronic applications are envisaged, in the final status the graphene layer has to be on an insulating substrate and to fully exploit the exciting electronic properties of this material, has to be patterned on the nanometer scale. Moreover, this patterning has to be carried out with a precise control of the crystallographic orientation [26,27]. Standard lithographic procedures like e-beam lithography are unable to accomplish the control of the crystallographic orientation and to yield graphene nanoribbon (GNR) widths in the range of nanometers [28–30]. The width of GNRs produced by anodic oxidation under the AFM tip, seems also to be limited in the range of 50 nm, and to date without achieving crystallographic orientation control [31]. Additional, unwanted effects arise from edge irregularity [30]. To date, the only technique able to achieve simultaneously the crystallographic orientation control and the size control of GNRs of nanometer widths is scanning tunneling lithography (STL) [32]. Other methods possibly offering crystallographic orientation control of the etched GNRs, or other nanopatterns, can be divided in two categories: (i) methods based on nanoparticle induced patterning [33,34], (ii) methods based on controlled oxidation [35]. The methods in both later categories relay on the selective chemical reaction for the removal of C atoms from the edge of the graphene sheet, therefore the crystallographic control is related to the different reaction rates of C atoms in zig-zag, or armchair positions. The aim of the present review is to analyze the status and possibilities of the methods providing crystallographic orientation control of the GNR edges.

2. Edge effects and disorder

The electronic structure and transport properties of GNRs are strongly affected by edge disorder. When producing any kind of nanopattern, as the relevant elements of such a pattern themselves are of atomic dimensions, the atomic structure and the regularity, or irregularity of the edges are of great importance. This is very similar to the importance of surface effects in thin films and nanoparticles: the thinner the film (smaller the particle), the more important the processes taking place in its surface will be. Similarly, the narrower the GNR, the edge effects will be more significant. The effects of the edge structure and its regularity, or irregularity on the electronic properties of graphene were extensively reviewed recently by Castro Neto et al. [20]. Additionally, effects arising from disorder, point defects, bending on the substrate roughness and electron scattering due to ripples, scattering produced by topological defects, cracks, and other topics are discussed in detail. All these structural imperfections have influence on the electronic and transport properties of graphene. Experimental confirmation of the effects arising from edge irregularity was reported by Özyilmaz et al. [36]. The fractional plateaus in the quantum Hall conductance arising from chiral edge states were used to probe the disorder of the edges of the GNR. The lack of quantization for the plateaus at Landau level filling factors ν', $\nu = \pm 2$ was interpreted as the consequence of electron backscattering between opposite edges of the samples. Temperature dependent conductance measurements show larger energy gaps opening for narrower ribbons, however the crystallographic orientation of the GNRs was not known as they were realized by e-beam lithography [28]. In an experiment designed to check the relative orientation dependence of the gap of GNRs etched from the same graphene flake, no characteristic dependence was found [28]. This shows that in the case of GNRs produced by e-beam lithography edge disorder may mask the effects of crystallographic orientation predicted by theory [20,37]. This finding is in agreement with theoretical results that in the case of a random edge, which is neither zig-zag, nor armchair, the zig-zag boundary conditions will be dominant in the Dirac equation [38]. The edge states in the zig-zag segments of a H terminated mixed edge are clearly evidenced by scanning tunneling microscopy/scanning tunneling spectroscopy (STM/STS) data acquired in UHV, such states are absent on the armchair edges [39]. Atomic resolution STM images show that point defects occurring at the zig-zag [39,40] and armchair edges [40,41] may perturb the electronic structure on distances of the nanometer magnitude inside the graphene flake. The effects arising from edge irregularity were investigated using single electron transistors (SET) in bottom and top gated GNRs [29]. It was found that disorder-induced islands within which the carriers are confined may be five to tens times longer than the width of the GNR. This was attributed to Anderson localization, due to strong scattering at the rough ribbon edges. A recent theoretical investigation of various types of defect configurations occurring both in zig-zag and armchair GNRs [42] has shown that depending on the specific edge disorder profile, defect density and ribbon symmetry, strong transport fluctuations may arise. These result in large mobility gaps or robust quasi-ballistic transport. It was found that these features are connected with the topology of edge irregularities as well as their correlation degree. For a certain defect density and termination, even a slight difference in the disorder profile can drive the system from a quasi-ballistic to a localized transport regime [42].

The above findings very clearly show that the edges of the GNRs have to be controlled with high precision. It is doubtful that the desired precision of the crystallographic orientation and satisfactorily defect free edges could be achieved by the widely used lithographic techniques, like e-beam lithography. Therefore new, dedicated lithographic processes have to be developed, which will be able to properly control the crystallographic orientation of the ribbon edges and their atomic structure as well.

3. Lithography with crystallographic orientation control

In order to be able to carry out lithography with crystallographic orientation control, either the crystallographic axes of the object have to be known with high precision – for a process that does not possess crystallographic selectivity – or the lithographic process itself has to possess crystallographic selectivity. In the former category one can enumerate the scanning probe microscopy-based lithographic processes, while in the second category one finds the various processes based on chemical reactions taking place at mobile nanoparticles. Although the movement of these nanoparticles cannot be controlled at our present level of knowledge, further research may reveal means to achieve this.

3.1. *Scanning probe microscopy (SPM)-based lithography*

The STM [43] and the atomic force microscope (AFM) [44] are known to be able to achieve atomic resolution imaging of flat surfaces. A recent review on the application of SPM lithography enumerates the vast extent of the various scientific and technical fields in which these techniques were used for lithography in almost three decades since their invention [45].

3.1.1. *Scanning tunneling lithography (STL)*

When the STM tip is brought within ~1 nm distance to the conducting sample, electrons start to tunnel between the tip and sample if an external bias in the range of 0.1 to a few volts is applied. Due to the particular physics of this quantum phenomenon [46] the tunneling current will have an exponential dependence on the magnitude of the gap separating the tip and the sample. This will have profound effects on the width of the tunneling channel, too. Practically, 90% of the current will flow between the tip atom on the apex and the sample atom over which the tip is positioned. Beyond making possible atomic resolution imaging, this confinement of the tunneling current offers unprecedented resolution to modify the sample surface. If the sample is flat, like graphene, then even the mechanically prepared tips, i.e., tips which have a random surface with spikes, will be most frequently quite satisfactory. Due to the exponential dependence of the tunneling current on the tip–sample distance, the atom closest to the sample will be automatically selected and the next row of atoms, as a rule of thumb, has a ten times reduced contribution to the tunneling current.

Already in 1985 the STM was used for nanometric lithography [47]. As HOPG is the workhorse of STM experiments in air, attempts to modify its surface by the STM tip started quite early [48]. In these first experiments it was already revealed that the writing of holes with a few nanometers in diameter is possible only in the presence of water vapor condensed on the surface of HOPG [48]. Later it was proposed that in fact, a localized chemical reaction takes place under the STM tip, Fig. 1, by the local decomposition of water under the well confined electron flux emitted from the tip [49]. The proposed reaction can be written as

$$C + H_2O \Rightarrow CO + H_2 + 2e^-. \quad (1)$$

The etching process of the surface of HOPG according to Eq. (1) depends on several factors [50]: (i) there is a certain threshold voltage in the range of a few volts, over which the modification of the sample surface starts; (ii) the magnitude of the threshold voltage depends on the scanning speed used;

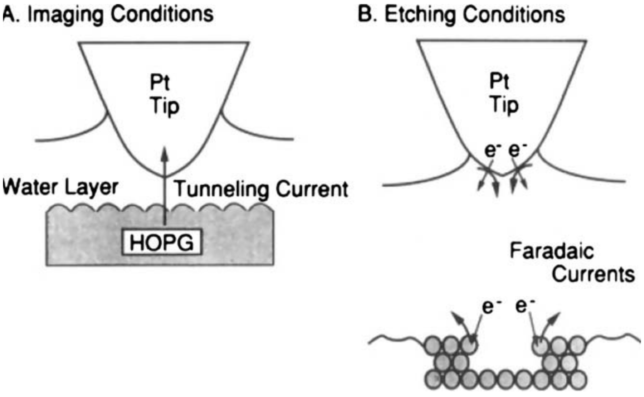

Fig. 1 – Schematic presentation of the STM tip, the HOPG sample, and the liquid water meniscus between the tip and sample. Under etching conditions the electrons launched from the STM tip at higher bias (typically a few volts) will decompose the water molecules according to Eq. (1) (see text). (Reproduced with permission from [49] Copyright 2010 American Chemical Society.)

(iii) in turn the width and the depth of the lithographic features depends on the applied bias. In a systematic study [50] it was shown that when keeping all other parameters constant except the bias voltage, the character and magnitude of the surface modifications changes significantly in the voltage range from 2.74 to 3.47 V. At the lower value, the first surface modifications were observed: small elevations on the sample surface, which are tentatively identified with C(O) type structures anchored to the sample surface. At the value of 3.47 V, the etching was already several atomic layers deep.

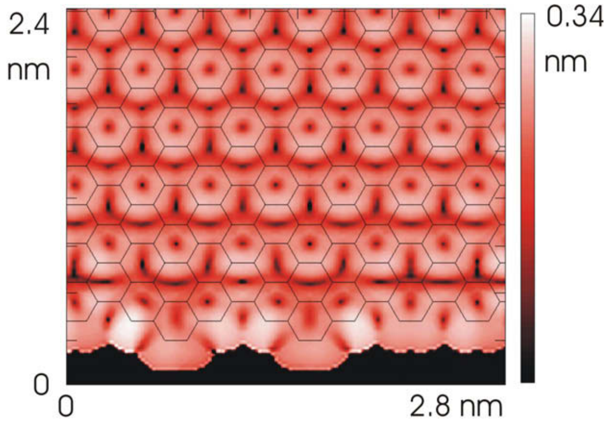

Fig. 3 – Computed STM image of an armchair GNR with imperfect edges for a ribbon with overall width of 4.18 nm. One can clearly observe localized electronic states on the atoms that belong to small zig-zag portions of the edges, especially at the center of these portions. Even with this perturbation present the experimentally observed stripes are clearly observed running parallel to the ribbon axis.

With a very careful tuning of the above parameters the cutting of GNRs only one layer thick is possible [32]. Using a 2.4 V bias potential and 2.0 nm/s tip velocity on the HOPG surface in air, GNRs with suitably regular edges were cut, which constitutes a great advance towards the reproducibility of GNR-based devices. The crystallographic orientation of the GNR was fixed after acquiring atomic resolution images of the sample surface. After the completion of the lithographic process the resulted GNR was imaged in atomic resolution with the same STM tip as used for lithography, Fig. 2. STS was used to probe the electronic structure of the GNRs, a confinement induced gap of 0.18 eV was found for the 10 nm wide armchair GNR in Fig. 2. As shown in the figure, it is clearly visible that the confinement of the electronic waves produces a standing wave pattern which is superimposed on the atomic resolution image of the GNR. In Fig. 2b the different periodicities are shown for an atomic resolution image and for the standing wave pattern. Such standing wave patterns are predicted by tight-binding theoretical calculations as shown in Fig. 3 even for an irregular edge armchair GNR of 4.18 nm in width. A similar tight-binding formalism was used as applied previously in computing the STM atlas of various single wall carbon nanotubes [51]. It was found that the particular stripe pattern is influenced by the width of the GNR and the character of the deviation from the ideal armchair edge, nevertheless the stripe pattern parallel with the ribbon axis is present in most investigated cases. Of course,

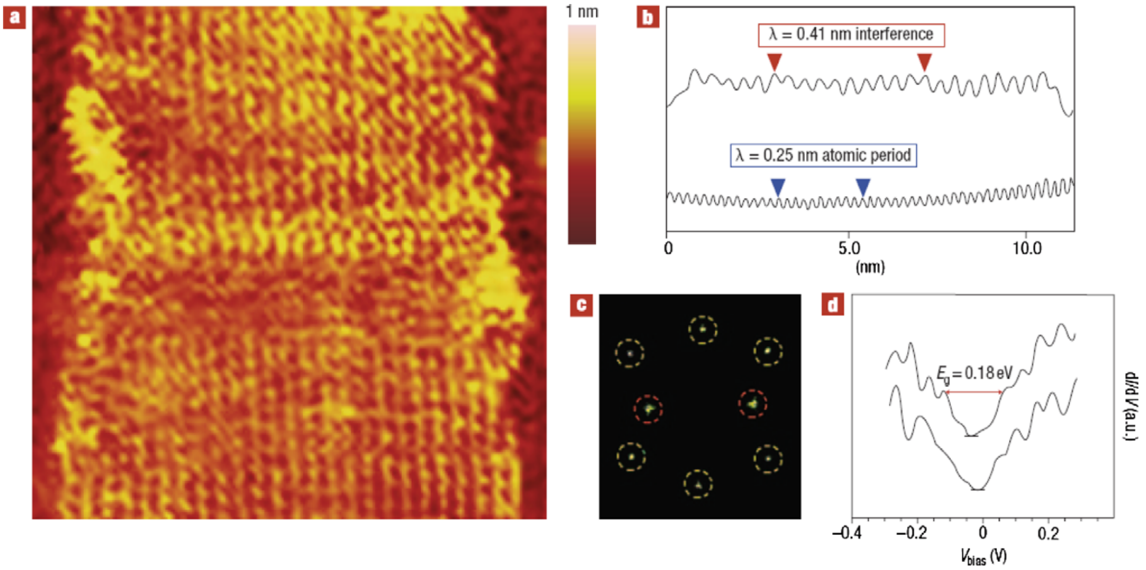

Fig. 2 – Topographic STM image and electronic structure of a GNR. (a) Constant-current STM image (12 × 12 nm^2, 1 nA, 100 mV) of a 10-nm-wide armchair GNR displaying confinement induced standing electron wave patterns (stripes parallel to the axis of the ribbon). The color scale bars encodes the height of the imaged features. (b) Average line-cuts revealing the period of the observed oscillation, which clearly differs from the periodicity of the underlying atomic structure. (c) 2D Fourier transformation of the STM image: the six dots in the apexes of the hexagon are produced by the atomic arrangement, the two extra dots, circled in red arise from the vertical stripes due to the electronic standing wave pattern. (d) Representative tunneling spectra (STS) taken on the ribbon, revealing an energy gap of 0.18 eV (zero density of states (DOS) marked by horizontal lines, the two spectra taken at different locations are shifted for clarity). (Reproduced from [32].) (For interpretation of the references to colour in this figure legend, the reader is referred to the web version of this article.)

the clearest pattern is found for a regular armchair edge (see Fig. 4 in [32]).

The confinement induced gap scales with ribbon width as predicted by theory. The narrowest armchair GNR of only 2.5 nm (about 10 benzene rings width) exhibited in the STS data taken at room temperature a gap of 0.5 eV [32]. This value is close to the gap of germanium and it clearly allows room temperature operation of nanoelectronic devices built of GNRs.

It may seem that the STL has a serious drawback: the sequential lithography of complex circuitry may take an unrealistically long time. Fortunately this bottleneck could be eliminated by the development of multitip instruments like the Millipede [52] or Dip Pen Nanolithography [53], operating with several hundreds or thousands of tips in parallel, this could allow massively parallel STL lithography. The patterns to be cut could be decomposed in elementary blocks, which could be cut by the various tips in a similar fashion like the old dot matrix printers printed complex patterns with a limited number of dots.

As double layer GNRs also seem to present interesting properties, STL may be a technologically realistic solution for writing complex patterns composed of elements of one, two, or several layers. As shown by recent results, STM is not only able to cut in the HOPG at a predetermined depth, but it can also manipulate single graphene layers, Fig. 4, while the narrowest two layers deep trench written being of 4.5 nm width [54]. The cutting depth can be precisely regulated by the properly chosen bias and scanning speed.

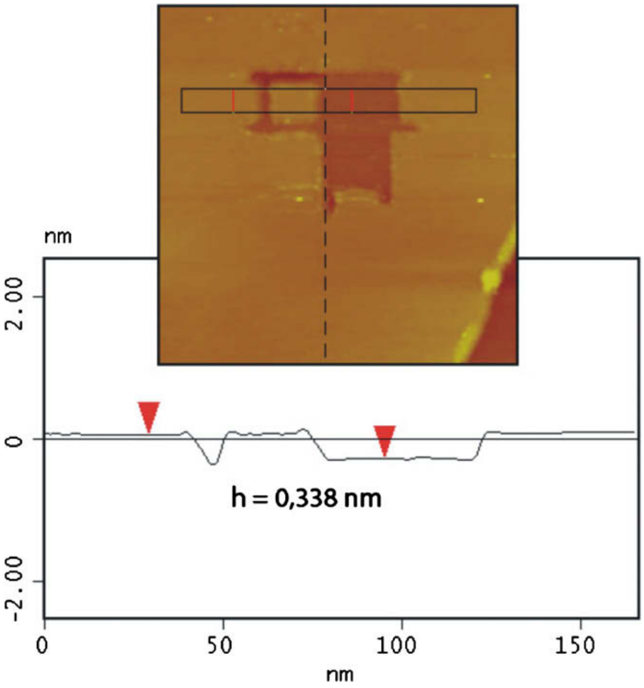

Fig. 4 – Topographic STM image consisting of three square features with one graphene layer thickness. Two of the squares have been removed. One may remark from the averaged cross section in a direction normal to the trench originally separating the top left square from the top right square that the bottom of the depression is as flat as the unperturbed top layer produced by cleavage. (Reproduced from [54].)

To date, STM is the only tool that can achieve simultaneously, within the same instrument and the same experiment, four major requirements of nanometer scale lithography of GNRs: (i) atomic resolution imaging; (ii) nanometer scale modification of one single layer of graphene; (iii) imaging the produced nanoobject in atomic resolution; and (iv) probing the electronic structure of the resulted nanoobject [32]. It is an important additional advantage that the method is resist free.

3.1.2. *AFM lithography by anodic oxidation*

AFM is also capable of acquiring atomic resolution images of the HOPG surface both in contact [55] and in non-contact mode [56]. Two refinements have to be made to the previous statement: on one hand, contact mode AFM (CM-AFM) is not exactly imaging the one single atom details (opposite to STM), due to the large tip radius it averages the atomic interactions, and it will not detect point defects observed in STM [55]. On the other hand, non-contact AFM (NC-AFM) images also do not image the individual C atoms on the graphite surface, image inversion will be present as showed by the comparison of experimental and computed AFM images and the center of the hexagon will appear as a bright spot on the NC-AFM images [56]. To date, no successful attempt was reported to use atomic resolution AFM images to control the crystallographic orientation of the GNRs produced by AFM lithography.

Conductive tip CM-AFM was successfully used to cut through multiwall carbon nanotubes (MWCNTs) on a HOPG substrate [57]. The cutting was possible only in negative tip bias regime, as in the case of STL discussed above. Similar behavior: a threshold voltage value and the increase of this threshold voltage with the increasing scan velocity were reported, as in the case of STL. As the magnitude of the bias voltage increased, the etch depth of the graphite surface increased exponentially and reached 7.9 nm, a thickness of 23 atomic layers of graphite, at a bias voltage of −10 V [57]. A cutting mechanism based on the field-emission current density of the Fowler–Nordheim equation was proposed: both the MWNT cutting and graphite etching encounter the same reaction where the activation energy is supplied by electrons that are field emitted from the negatively biased AFM tip. On the other hand the AFM was operated in ambient atmosphere with a relative humidity of 40–70%. So very likely, similar processes took place as in the case of STL lithography.

A recent study reported conductive tip CM-AFM nanomachining of HOPG both with a metal-coated Si tip and with a carbon nanotube tip [58]. With the metal-coated Si tip it was possible to fabricate holes as small as 10 nm in diameter and 0.34 nm depth. For this −8 V pulse was applied to the metal-coated tip with 50 ms pulse width (50% duty ratio), 300 repetition times. *I*–*V* curves acquired in contact mode, with scanning disabled did not confirm Fowler–Nordheim field emission, it was conclude that the etching process is similar to the case of STL. When using MWCNT tips, the MWCNT was bent during the hole formation process and due to slipping on the sample surface it produced trenches instead of holes. For a certain depth the trenches written with the

MWNT tip had a higher aspect ratio than the trenches written with the metal-coated Si tip. By AFM local oxidation patterning GNRs with a width down to 25 nm were produced on SiO_2 [59] Fig. 5. Negative tip bias in the range of 15–30 V was used and both the topographic characterization and lithography was carried out with a conductive Si tip in non-contact (tapping) mode under ambient conditions. The bias voltage is modulated between zero and the set value with a 100 Hz square wave to help stabilize a water meniscus around the tip. The apparent height of the graphene flake in Fig. 5 is of the order of 1 nm, this may mean that it is composed of several graphene layers, or that the conditions of the NC-AFM imaging were not properly chosen [60]. Surprisingly, for certain experimental conditions hole or trench formation was observed for both positive and negative tip biases. For a certain voltage and set point combination, bumps not trenches were formed [59]. This may be related to deposition of material from the tip.

GaAs substrates were used instead of thermally grown SiO_2 on Si in experiments to manipulate single graphene layers by the AFM [61]. The main advantage of the atomically flat substrate is a better adherence of the few layer graphite and graphene as compared with the rougher SiO_2. This allows the mechanical structuring of the few layer graphite (FLG) under CM-AFM tip. The anodic oxidation of the graphene covered by the adsorbed water film (controlled humidity of 55–60%) under the AFM tip was carried out on oxidized Si substrates using a constant negative tip bias of 27 V and a tip velocity of 0.05 μm/s [61]. The width of the oxidized grooves typically varies between 30 and 100 nm, mainly depending on the apex of the used AFM tip, and thereby defines the limit on the resolution possible with this technique.

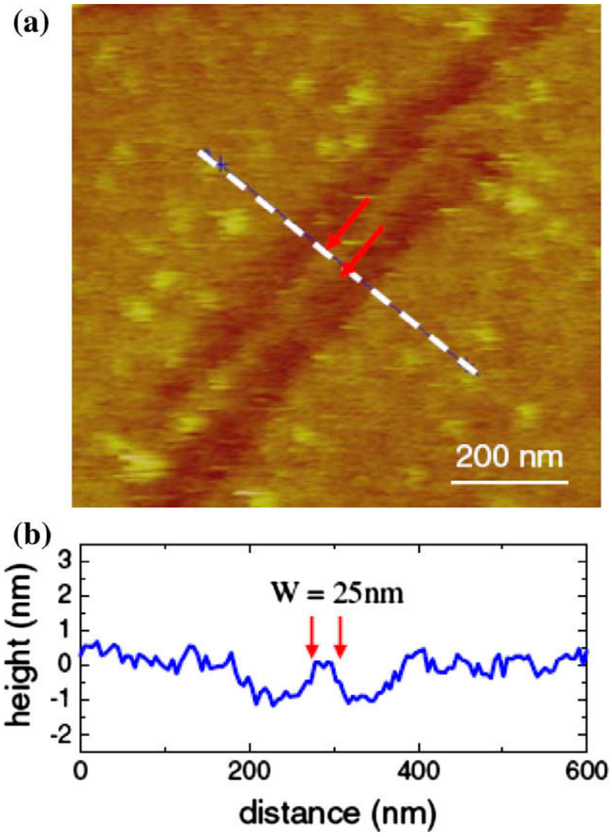

Fig. 5 – (a) AFM image of a nanoribbon fabricated on a graphene flake. The width and length of the ribbon are 25 and 800 nm, respectively. (b) Height profile along the dashed line in (a). (Reproduced with permission from [59] Copyright [2010], American Institute of Physics.)

In summary: although the processes taking place are similar to those occurring during STL, due to the larger radius of curvature of the AFM tips, the resolution of the AFM-based anodic oxidation lithography is not likely to improve below the range of 20–30 nm. This and the lack of crystallographic orientation control do not offer clear advantages as compared with e-beam lithography.

3.2. *Chemical reactions with crystallographic selectivity*

3.2.1. *Reactions of mobile nanoparticles*

Several kinds of metallic nanoparticles were reported to cut one or several layers deep trenches in graphite in selected crystallographic directions: Ni [33,62], Fe [63], and Co [64,65] when heated in a hydrogen containing atmosphere. In certain experiments even GNRs of 10 nm in width were observed. Ag nanoparticles promote the oxidation of graphene [66]. Very recently SiO_x nanoparticles were also reported to behave in a similar way like the transition metals [67]. The SiO_x nanoparticles were produced in situ by the annealing of graphene on SiO_2 in hydrogen containing atmosphere at temperatures over 850 °C.

3.2.1.1. Hydrogenation at mobile nanoparticles. In some sense the chemical processes taking place at the mobile transition metal nanoparticles can be regarded as the opposite reaction that takes place during CVD carbon nanotube (CNT) growth [68]. While during CNT growth the reaction equilibrium is shifted towards hydrocarbon decomposition and carbon precipitation on the surface of the catalytic nanoparticles, in the hydrogenation process the solid carbon is consumed at the location where the catalytic nanoparticle is in contact with it. This process is known as “gasification” (see Ref. [33] and references therein). The fact that most often the nanoparticles do not burrow into the graphite substrate, but follow the receding graphene layer, indicates that on one hand dangling carbon bonds are needed for the reaction to take place [65], on the other hand, the position of the nanoparticle when in contact with a graphene step is energetically favorable over the position on the flat basal plane of graphite. This may be the source of the driving force that makes the nanoparticle to become mobile.

In fact, the so called hydrogenation reaction of graphite has been extensively studied previously (see. Ref. [64] and references therein). It was found that the reaction between graphite and hydrogen was strongly catalyzed by iron, cobalt and nickel; however, control of the channeling has not yet been successful [69]. Unfortunately, the several decades long history of the cutting process by transition metal nanoparticles and the persistent lack of control on the starting point and orientation of the cut, may make uncertain its applicability to practical graphene nanolithography. Unless, the more recent efforts [33,62–67] will yield ways to fully control the cutting of graphene layers by the mobile nanoparticles.

The hydrogenation reaction of graphite at transition metal nanoparticles yields methane, but the precise catalytic mechanism is still debated [64,65]. The detailed HR-TEM investigation of the Co catalytic particles revealed that the part of the particle in contact with the graphite layers is always hcp Co, but the tail contains oxides, too: CoO and Co_3O_4 [65]. After annealing in vacuum the Co nanoparticles are encapsulated in a graphitic shell [65].

In the hydrogenation experiments by in situ formed SiO_x nanoparticles, the particles were formed from the SiO_2/Si substrate at the edges of the FLG flakes. Their composition was investigated by high resolution XPS, no metals were evidenced and the composition of the in situ formed nanoparticles was found to be SiO_x [67]. The hydrogenation mechanism proposed is similar to that of metallic nanoparticles, quantum size effects are assumed to be responsible for this [67].

Presently the most frequently used techniques of precisely placing nanoparticles on a surface [70] can be grouped as detailed below: (i) those involving chemical, or biological templates, this is not desirable in the case of graphene as it will result in unwanted residues; (ii) methods based on trenches, these are unsuitable for graphene because of geometric reasons; (iii) capillary-force-driven assembly, which needs the 3D structuring of the surface and (iv) methods using fields to manipulate the nanoparticles. The resolution of the later methods is in the range of 6 nm [71] and guiding electrodes have to be present on the surface. If no such methods are involved the particles will be placed at random, which is unsuitable for producing a preplanned pattern.

3.2.1.2. *Oxidation at mobile nanoparticles.*

For the catalytic oxidation by Ag nanoparticles the proposed reaction mechanism is based on O_2 adsorption and dissociation on the surface of the Ag nanoparticle, followed by the diffusion of atomic O to the graphene edge where CO and CO_2 formation takes place [66]. Straight and "spiraling" channels were equally observed, the later type of channel was not reported in channeling by transition metal nanoparticles. Apparently, the switchover from relatively straight segments to spiraling ones occurs randomly.

Similarly to the hydrogenation at mobile particles, the catalytic oxidation of graphite at various metal oxide nanoparticles was also investigated since the seventies of the previous century, Ref. [65] and references therein. In particular, the study of the catalytic oxidation in the presence of Ag showed that the behavior of the catalyst depends on the initial heating rate [72]. At slow heating rates atoms are extracted from perfect regions of the basal plane surface to produce pits, and channels which do not start at edges. At high heating rates only channels are formed which start at edges.

3.2.1.3. *Summary of the recent experiments.*

Table 1 summarizes the conditions used in recent patterning experiments of graphene, FLG and HOPG. The general conclusions of these experiments can be formulated as follows: (i) the pattern formation is attributed to a localized chemical reaction catalyzed by some kind of mobile nanoparticle; (ii) the driving force for the movement of the nanoparticle arises from its more favorable energetic position when in contact with edges of the graphene or FLG channel; (iii) clear crystallographic selectivity is found for 30°, 60°, and 120° direction changes, but apparently there are not significant differences between transition metal, and SiO_x nanoparticles in hydrogenation experiments, and/or oxidation at Ag nanoparticles as it regards the possibility to control the starting point of the etching ant its direction. This last finding together with the four decades history of the field may question if these methods will be indeed suitable for well controlled lithographic processes. On the other hand, the comparison of graphene and HOPG etching by Ni nanoparticles, Fig. 6, indicates that the processes may be somewhat dependent on the nature of the layer below the topmost graphene layer [62]. It is reported that when etching one single layer of graphene on SiO_2 all cuts are oriented with the same edge chirality and the cuts do not cross each other, in contrast to the same process in graphite. [62]. Earlier reports indicate that the chemical reactivity of armchair and zig-zag edges is different [73,74], at present there is a lack of data on the orientation of the edges produced by Ni etching of graphene on SiO_2.

A point should be emphasized here: the characteristic angles by which the trenches etched by mobile nanoparticles change direction indicate that the reactivity of graphene, FLG and graphite is different along different crystallographic directions in the basal plane. This will be used later for the discussion of pattern formation by controlled oxidation.

3.2.2. *Controlled oxidation of graphene on SiO_2 with crystallographic selectivity*

As it was discussed in the previous section, under certain annealing conditions the graphene may interact with its sub-

Table 1 – Table summarizing the experimental conditions of recent experiments for cutting graphene, FLG, and HOPG layers by mobile nanoparticles.

Nanoparticle	Etched material/substrate	Atmosphere	Temperature (°C)	Reference
Ni	HOPG	Ar/H_2 (85/15 by volume)	750–1100	[33]
Ni	Graphene/SiO_2	Ar/H_2 (850 sscm/150 sscm)	1100	[62]
Fe	FLG/SiO_2	Ar/H_2 (600 sscm/320 sscm)	900	[63]
Co	HOPG	N_2/H_2 (90/10 by volume)	700	[64]
Co	HOPG	H_2 (60 mbar)	400–900	[65]
Ag	HOPG	Ambient air	650	[66]
SiO_x	FLG/SiO_2	H_2 (40 sccm)	850–1100	[67]

FLG: few layer graphite.

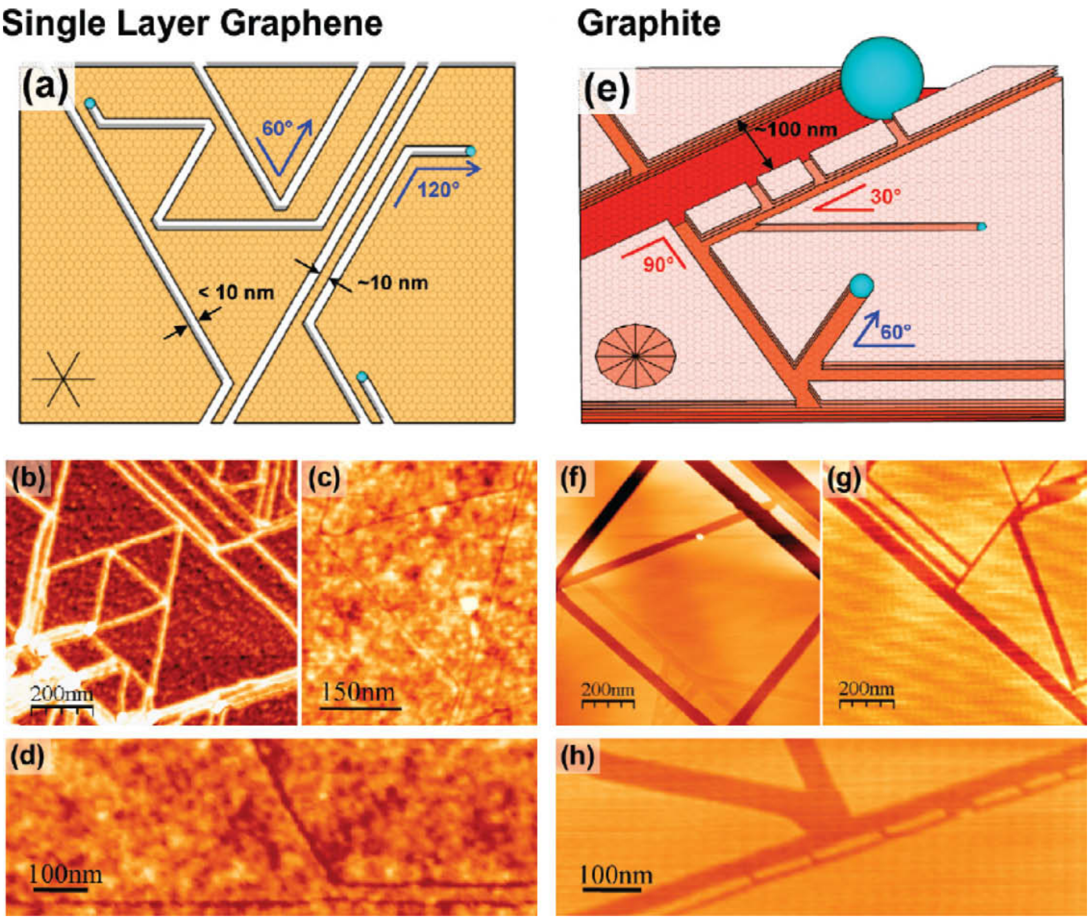

Fig. 6 – Comparison of nanoparticle-assisted etching in SLG and graphite. (a) Key features of etching in SLG are chirality-preserving angles of 60° and 120°, avoided crossing of trenches leaving ~10 nm spacing between adjacent trenches and producing connected nanostructures, and trenches and nanoparticles with uniform width <10 nm. (b) AFM phase image of etched SLG with produced geometric nanostructures. The phase image obscures small details, making adjacent trenches appear to merge together. (c) AFM height image of equilateral triangle connected to three nanoribbons. (d) AFM height image of a trench which avoids crossing another trench, running parallel to it (panels c and d color scale 0–1.7 nm). (e) Key features of etching in graphite and few layer graphene are chirality-changing angles of 90°, 150°, and 30°, in addition to 60° and 120°, trenches which merge, producing disconnected geometries, and trenches and nanoparticles of varying size (10–1000 nm). (f–h) AFM height images of etched graphite showing the previously mentioned features (color scale 0–7 nm). (Reproduced with permission from [62] Copyright 2010 American Chemical Society.) (For interpretation of the references to colour in this figure legend, the reader is referred to the web version of this article.)

strate to produce chemical reactions [67]. It was observed during the oxidative thinning of FLG flakes down to a single layer of graphene: when a certain region of the sample reaches the monolayer thickness, its interaction with the substrate changes [75]. The edges of the graphene layer recede in a way that they leave behind a depression, see Fig. 2d in Ref. [75]. This is in agreement with earlier observations that SWCNTs produce trenches on the SiO_2 surface [76]. As no dip formation was observed at the edges of the FLG flakes, this indicates that the consumption of the SiO_2 substrate may be a reaction specific to graphene. In a subsequent work in which graphene flakes were produced by mechanical exfoliation it was found that the consumption of the SiO_2 substrate at the receding graphene edges takes place during annealing in a pure Ar atmosphere at the temperature of 700 °C, too [77]. Under these conditions the oxidation takes place only at the already existing graphene edges according to the reaction:

$$SiO_2(sol) + C(sol) \Rightarrow SiO\uparrow + CO\uparrow. \qquad (2)$$

As both reaction products are volatile at the annealing temperature, they are removed by the Ar flux, therefore a depression is created where the graphene edge has reduced the substrate silica to SiO. The reaction is a solid phase reaction which exhibits clear signs of crystallographic selectivity. The initially round shape of the pits formed during the oxidation of the graphene at 500 °C in air is converted to a well shaped, regular hexagon, Fig. 7. By atomic resolution STM measurements it was possible to show that the edge orientation of the hexagonal holes is zig-zag [77]. Raman spectroscopy unambiguously confirmed that the controlled etching in Ar did not increase the defect level of the graphene layer [77].

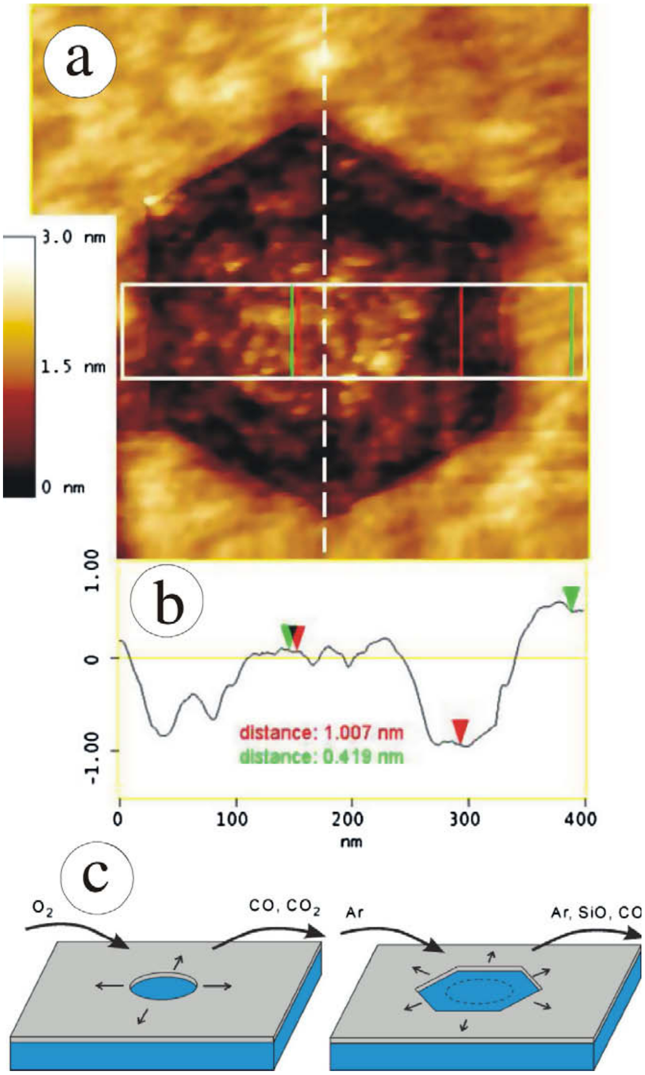

Fig. 7 – AFM image of a hexagonal pit obtained after etching in Ar atmosphere. (a) Tapping mode AFM image of the hexagonal etch pit. The white rectangle marks the area where an averaged height profile has been obtained. Notice the very sharp and well defined edges of the etched graphene. (b) Averaged line cut over the marked area in (a). (c) Schematic illustrating the first (air) and the second (Ar atmosphere) etching processes. (Adapted from [77].)

The starting point of the etching reaction can be precisely predetermined by AFM indentation. It this way very complex patterns can be etched using the hexagonal holes as "building blocks". As a demonstration the first Y-junction composed of zig-zag GNRs was produced [77]. It is worth to emphasize that the procedure has several advantages: (i) it can be performed on SiO_2; (ii) it is completely resist free; (iii) it generates a well defined edge orientation; (iv) it is compatible with standard integrated circuit technology.

4. Edge "engineering"

As it was already discussed in Section 2, the quality and the regularity of the GNR edge is of paramount importance. The above survey of the crystallographically selective/controlled lithographic techniques showed that it may not be a simple task to achieve simultaneously the precise control of the location where the etching starts, of the crystallographic orientation of the GNR, and in the same time to obtain highly regular edges. Therefore it may be useful to separate the crystallographically controlled lithography and the edge engineering. In Section 3 several reactions were discussed which clearly exhibited crystallographic selectivity, these results indicate that the shaping of already formed graphene edges may be possible. Recently, several groups reported experimental results clearly showing that edge engineering is possible. However, there is some controversy: Koskinen et al. formulated theoretical [78] arguments for the reconstruction of both armchair and zig-zag edges with the incorporation of non-hexagonal rings, in particular pentagons and heptagons. On the other hand, clear armchair and zig-zag edges were evidenced in experiments reported in parallel in Refs. [72,79]. In a later paper, some experimental results of Ref. [80] were reinterpretated by Koskinen et al. [81], showing the presence of structures in which the predicted reconstruction [78], Fig. 8, could be observed in aberration-corrected transmission electron microscope images. They propose for this type of reconstructed edge the term of "reczag" edge and bring arguments that it should be thermodynamically stable [81]. However, one should keep in mind that the images were obtained under dynamic conditions of continuous electron bombardment, which may influence the stability of a certain edge structure. The existence of the reczag edge may have several important implications [81]: (i) it may reduce edge stress; (ii) it has similar vibrational properties like the armchair edge, this may lead to erroneous identifications; (iii) it influences the transport properties; and last, but not least, (iv) it is chemically less reactive than a zig-zag edge.

In heating experiments carried out inside a combined TEM-STM microscope it was found that by applying Joule heating, the originally irregular edges of a CVD grown graphitic nanoribbon were transformed in armchair and zig-zag edges [79]. The mechanism of reconstruction or crystallization for the nanoribbons and edges is attributed primarily to the carbon atom vaporization, the current flow along the ribbon and edges, and the high temperature associated with the resistive Joule heating. Transformations from AA stacking to the ABAB (Bernall) stacking were observed during heating, suggesting that the sample reached temperatures in the range of 2000 °C. Longer time heating of the same region revealed that under the conditions of the experiment, the zig-zag type edges tend to join with the evaporation of armchair edges separating them, Fig. 9, [79]. The edge motion mostly follows either zig-zag or armchair crystallographic orientations, and the speed of edges moving along the heat flow direction is higher (2 nm/min) than that along the current flow direction when the two are antiparallel (1 nm/min). Edge motion along other directions is not favored. Here, one also should keep in mind that the experimental data were acquired under conditions very far from equilibrium.

Using a transmission electron aberration-corrected microscope, in high vacuum environment, capable of simultaneous atomic spatial resolution and 1-s temporal resolution, movies of the dynamics of carbon atoms at the edge of a hole in a

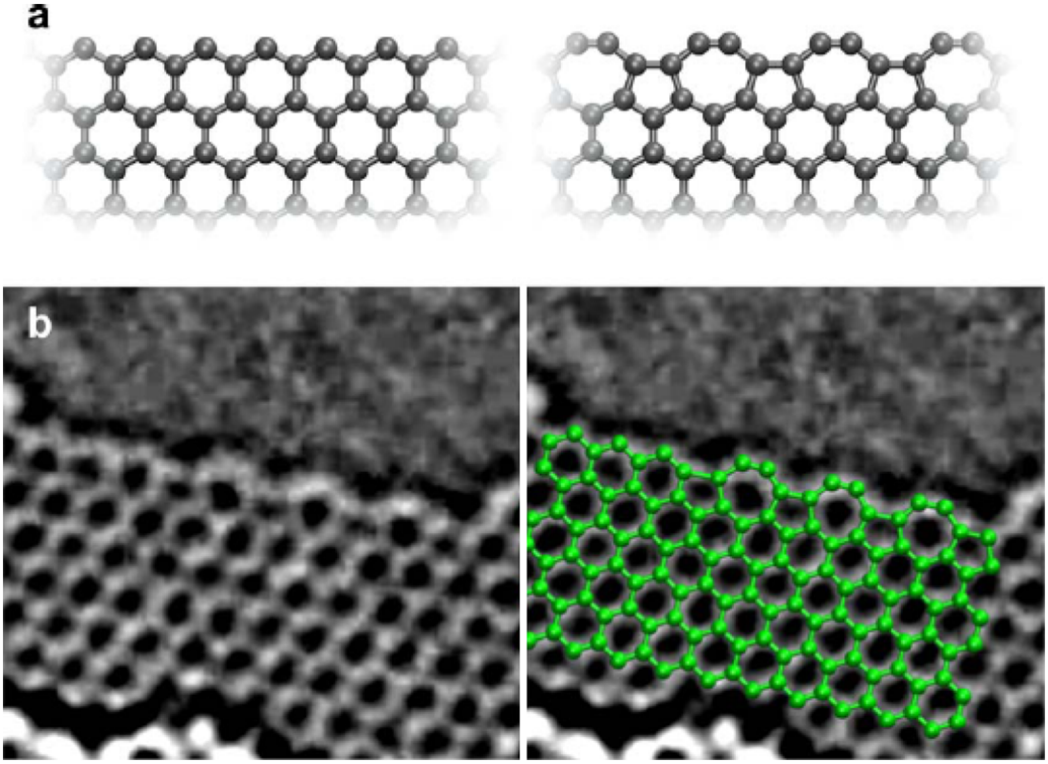

Fig. 8 – Structure of the reczag edges. (a) Left: regular zig-zag edge, right: reconstructed reczag edge. (b) Left: TEM image showing a zig-zag edge that continues into a reczag edge, right: atomic structure overlayed on the image at left. (Reproduced with permission from [81] Copyright (2010) by the American Physical Society.)

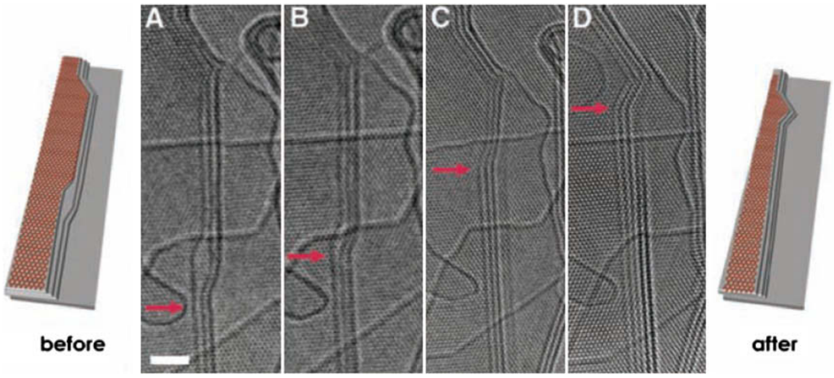

Fig. 9 – Evolution in time of an edge from a mixed armchair/zig-zag/armchair/zig-zag status (left) to pure armchair/zig-zag/zig-zag structure (right). The red arrows marks the movement of the zig-zap portion intercalated between two armchair edge regions, reproduced with permission of the AAAS from [79]. (For interpretation of the references to colour in this figure legend, the reader is referred to the web version of this article.)

suspended, single atomic layer of graphene were produced [80]. The rearrangement of bonds and beam-induced ejection of carbon atoms were recorded as the hole grew. Prolonged electron irradiation was used as source of energy input into the sample. The movies of time evolution indicate the higher stability of zig-zag edges [80]. As in the previous case, here too, the experimental conditions are far from equilibrium.

In a recent paper unexpected structures were revealed by HR-TEM on graphene edges: protruding hexagons on armchair edges and single C atoms bonded to zig-zag edges [82]. The specimens were thermally annealed but kept at room temperature during HR-TEM observation. The same effect, as reported in Ref. [79] was observed, namely that the irregular edges transform to straight edges during annealing. By tilting experiments it was shown that the edges of adjacent graphene layers most frequently are closed and that it is not straightforward to distinguish these edges from open double layer edges [82].

To summarize this section: several experiments carried out in various ways confirm that edge engineering of graphene is possible. On the other hand several new and to some extent surprising experimental and theoretical results suggest that the commonly assumed edge structures have to be reevaluated.

5. Summary and outlook

The review of the recent literature on the nanopatterning of graphene with the crystallographic control of the edge orientation shows that up to now the most successful way of preparing GNRs with well controlled crystallographic orientation was achieved by STM lithography (STL). The orientation of the GNRs was chosen on the basis of atomic resolution STM images, the nanoribbons were characterized both by atomic resolution STM images and STS. Their behavior is in agreement with theoretical expectations. The method has two drawbacks: (i) the need for a conducting substrate; and (ii) a certain degree of edge irregularity on the subnanometer scale. The later drawback could be avoided by edge engineering after the lithographic process was completed. An important advantage is that the STL process does not need the use of any resist.

The local oxidation of graphene under a conductive AFM tip in principle is similar to the STL method with two observations: (i) due to the much larger radius of curvature of the AFM tip as compared with an average STM tip the features cut are significantly wider; (ii) using the AFM feedback signal instead of the tunneling current (exponential dependence on tip sample distance!) also contributes to the loss of resolution. On the other hand, a clear benefit of the method is that it can operate on non-conducting substrates, too.

The lithography by mobile nanoparticles, although interesting, is a very complex process that was not fully elucidated in the past 40 years. Therefore, its rigorous control (starting point definition and predetermination of the cut direction) which is needed for GNR cutting is not very close.

The controlled oxidation of the graphene by the consumption of the SiO_2 substrate clearly exhibits crystallographic selectivity, the hole edges are of zig-zag orientation. The procedure has several advantages: (i) it can be performed on SiO_2; (ii) it is completely resist free; (iii) it generates a well defined edge orientation; (iv) it is compatible with standard integrated circuit technology. The method allows to “build together” complex patterns from hexagonal building blocks. The first GNR Y-junction was produced.

The possibilities of edge engineering may prove to be extremely useful for both STM and AFM lithography, provided that these methods offer the possibility of crystallographic orientation control. Presently these methods seem most suited to produce GNRs with well characterized orientation and edges if lithography is combined with postlithographic edge engineering. Perhaps, even width reduction could be achieved by careful edge engineering.

Finally, we should point out that despite the numerous theoretical works investigating various kinds of edge disorders and several experimental papers reporting transport measurements on GNRs, the experimental data on the transport of GNRs with known edge orientation and well characterized defects structure are still lacking. There is also a lack of information on comparing the properties of GNRs with the same edge orientation and similar width, but differing edge disorder. On the basis of these experimental data it would be possible to decide to what extent the much higher edge disorder induced by plasma etch after e-beam lithography, as compared to the edge disorder produced by STM lithography, is acceptable because of advantages offered by the better established technology of e-beam lithography.

Acknowledgement

The present work was supported in Hungary by OTKA grants K67793 and NI67851. LPB gratefully acknowledges the agreement between the FNRS and HAS that made possible the cooperation with PhL. Helpful discussion with Dr. ZE Horváth and Mr. P. Nemes-Incze are acknowledged.

REFERENCES

[1] Geim AK, Novoselov KS. The rise of graphene. Nat Mater 2007;6:183–91.
[2] Novoselov KS, Geim AK, Morozov SV, Jiang D, Zhang Y, Dubonos SV, et al. Electric field effect in atomically thin carbon films. Science 2004;306:666–9.
[3] Peierls RE. Quelques proprietes typiques des corpses solides. Ann I H Poincare 1935;5:177–222.
[4] Landau LD. Zur Theorie der phasenumwandlungen II. Phys Z Sowjetunion 1937;11:26–35.
[5] Boehm H-P, Setton R, Stumpp E. Nomenclature and terminology of graphite intercalation compounds. Pure Appl Chem 1994;66:1893–901.
[6] Boehm H-P, Setton R, Stumpp E. Nomenclature and terminology of graphite intercalation compounds. Carbon 1986;24:241–5.
[7] Lu X, Yu M, Huang H, Ruoff RS. Tailoring graphite with the goal of achieving single sheets. Nanotechnology 1999;10:269–72.
[8] Segal M. Selling graphene by the ton. Nat Nanotechnol 2009;4:612–4.
[9] Stankovich S, Dikin DA, Piner RP, Kohlhaas KA, Kleinhammes A, Jia Y, et al. Synthesis of graphene-based nanosheets via chemical reduction of exfoliated graphite oxide. Carbon 2007;45:1558–65.
[10] Li X, Wang X, Zhang L, Lee S, Dai H. Chemically derived, ultrasmooth graphene nanoribbon semiconductors. Science 2008;319:1229–32.
[11] Mkhoyan KA, Contryman AW, Silcox J, Stewart DA, Eda G, Mattevi C, et al. Atomic and electronic structure of graphene-oxide. Nano Lett 2009;9(3):1058–63.
[12] Wu Z-S, Ren W, Gao L, Liu B, Jiang C, Cheng H-M. Synthesis of high-quality graphene with a pre-determined number of layers. Carbon 2009;47:493–9.
[13] Jung I, Dikin DA, Piner RD, Ruoff RS. Tunable electrical conductivity of individual graphene oxide sheets reduced at “low” temperatures. Nano Lett 2008;8(12):4283–7.
[14] Tung VC, Allen MJ, Yang Y, Kaner RB. High-throughput solution processing of large-scale graphene. Nat Naotechnol 2009;4:25–9.
[15] Li X, Zhang G, Bai X, Sun X, Wang X, Wang E, et al. Highly conducting graphene sheets and Langmuir–Blodgett films. Nat Nanotechnol 2008;3:538–42.
[16] Hernandez Y, Nicolosi V, Lotya M, Blighe FM, Sun Z, De S, et al. High-yield production of graphene by liquid-phase exfoliation of graphite. Nat Nanotechnol 2008;3:563–8.

[17] Paredes JI, Villar-Rodil S, Solis-Fernandez P, Martınez-Alonso A, Tascon JMD. Atomic force and scanning tunneling microscopy imaging of graphene nanosheets derived from graphite oxide. Langmuir 2009;25(10):5957–68.
[18] Berger C, Song Z, Li T, Li X, Ogbazghi AY, Feng R, et al. Ultrathin epitaxial graphite: 2D electron gas properties and a route toward graphene-based nanoelectronics. J Phys Chem B 2004;108:19912–6.
[19] Hass J, de Heer WA, Conrad EH. The growth and morphology of epitaxial multilayer graphene. J Phys: Condens Matter 2008;20:323202-1–323202-27.
[20] Castro Neto AH, Guinea, Peres NMR, Novoselov KS, Geim AK. The electronic properties of graphene. Rev Mod Phys 2009;81:110–62.
[21] Obraztsov AN, Obraztsova EA, Tyurnina AV, Zolotukhin AA. Chemical vapor deposition of thin graphite films of nanometer thickness. Carbon 2007;45:2017–21.
[22] Reina A, Jia X, Ho J, Nezich D, Son H, Bulovic V, et al. Large area, few-layer graphene films on arbitrary substrates by chemical vapor deposition. Nano Lett 2008;9(1):30–5.
[23] Sutter PW, Flege J-I, Sutter EA. Epitaxial graphene on ruthenium. Nat Mater 2008;7:406–11.
[24] Li X, Cai W, An J, Kim S, Nah J, Yang D, et al. Large-area synthesis of high-quality and uniform graphene films on copper foils. Science 2009;324:1312–4.
[25] Wellmann R, Beottcher A, Kappes M, Kohl U, Niehus H. Growth of graphene layers on HOPG via exposure to methyl radicals. Surf Sci 2003;542:81–93.
[26] Barone V, Hod O, Scuseria GE. Electronic structure and stability of semiconducting graphene nanoribbons. Nano Lett 2006;6(12):2748–54.
[27] Son Y-W, Cohen ML, Louie SG. Energy gaps in graphene nanoribbons. Phys Rev Lett 2006;97:216803-1–4.
[28] Han MY, Özyilmaz B, Zhang Y, Philip Kim P. Energy band-gap engineering of graphene nanoribbons. Phys Rev Lett 2007;98:206805-1–4.
[29] Liu X, Oostinga JB, Morpurgo AF, Vandersypen LMK. Electrostatic confinement of electrons in graphene nanoribbons. Phys Rev B 2009;80. 121407(R)-1–4.
[30] Stampfer C, Güttinger J, Hellmüller S, Molitor F, Ensslin K, Ihn T. Energy gaps in etched graphene nanoribbons. Phys Rev Lett 2009;102:056403-1–4.
[31] Masubuchi S, Ono M, Yoshida K, Hirakawa K, Machida T. Fabrication of graphene nanoribbon by local anodic oxidation lithography using atomic force microscope. Appl Phys Lett 2009;94:082107-1–3.
[32] Tapasztó L, Dobrik G, Lambin Ph, Biró LP. Tailoring the atomic structure of graphene nanoribbons by scanning tunnelling microscope lithography. Nat Nanotechnol 2008;3: 397–401.
[33] Ci L, Xu Z, Wang L, Gao W, Ding F, Kelly KF, et al. Controlled nanocutting of graphene. Nano Res 2008;1:116–22.
[34] Datta SS, Strachan DR, Khamis SM, Johnson ATC. Crystallographic etching of few-layer graphene. Nano Lett 2008;8:1912–5.
[35] Nemes-Incze P, Magda G, Kamarás K, Biró LP. Crystallographically selective nanopatterning of graphene on SiO_2. Nano Res 2010;3:110–6. doi:10.1007/s12274-010-1015-3.
[36] Özyilmaz B, Jarillo-Herrero P, Efetov D, Abanin DA, Levitov LS, et al. Electronic transport and quantum hall effect in bipolar graphene p–n–p junctions. Phys Rev Lett 2007;99: 166804-1–4.
[37] Barone V, Hod O, Scuseria GE. Electronic structure and stability of semiconducting graphene nanoribbons. Nano Lett 2006;6:2748–54.
[38] Akhmerov AR, Beenakker CWJ. Boundary conditions for Dirac fermions on a terminated honeycomb lattice. Phys Rev B 2008;77:085423-1–085423-10.
[39] Enoki T, Kobayashi Y, Fukui K. Electronic structures of graphene edges and nanographene. Int Rev Phys Chem 2007;26:609–45.
[40] Niimi Y, Matsui T, Kambara H, Tagami K, Tsukada M, Fukuyama H. Scanning tunneling microscopy and spectroscopy of the electronic local density of states of graphite surfaces near monoatomic step edges. Phys Rev B 2006;73:085421-1–8.
[41] Kobayashi Y, Fukui K, Enoki T, Kusakabe K, Kaburagi Y. Observation of zigzag and armchair edges of graphite using scanning tunneling microscopy and spectroscopy. Phys Rev B 2005;71:193406-1–4.
[42] Cresti A, Roche S. Range and correlation effects in edge disordered graphene nanoribbons. New J Phys 2009;11:095004-1–095004-12.
[43] Binnig G, Rohrer H, Gerber C, Weibel E. Phys Rev Lett 1982;49:57–61.
[44] Binnig G, Gerber Ch, Quate FF. Atomic force microscope. Phys Rev Lett 1986;56:930–3.
[45] Tseng AA, Notargiacomo A, Chen TP. Nanofabrication by scanning probe microscope lithography: a review. J Vac Sci Technol B 2005;23:877–94.
[46] Tersoff. J, Hamann DR. Theory of the scanning tunneling microscope. Phys Rev B 1985;31:805–13.
[47] Ringger M, Hidber HR, Schlögl R, Oelhafen P, Güntherodt H-J. Nanometer lithography with the scanning tunneling microscope. Appl Phys Lett 1985;46:832–4.
[48] Albrecht TR, Dovek MM, Kirk MD, Lang CA, Quate CF, Smith DPE. Nanometer-scale hole formation on graphite using a scanning tunneling microscope. Appl Phys Lett 1989;55:1727–9.
[49] McCarley RL, Hendricks SA, Bard AJ. Controlled nanofabrication of highly oriented pyrolythic with the scanning tunneling microscope. J Phys Chem 1992;98:10089–92.
[50] Hiura H. Tailoring graphite layers by scanning tunneling microscopy. Appl Surf Sci 2004;222:374–81.
[51] Lambin P, Márk GI, Meunier V, Biró LP. Computation of STM images of carbon nanotubes. Int J Quant Chem 2003;95:493–503.
[52] Knoll A, Bächtold P, Bonan J, Cherubini G, Despont M, Drechsler U, et al. Integrating nanotechnology into a working storage device. Microelectron Eng 2006;83:1692–7.
[53] Haaheim J, Nafday OA. Dip Pen Nanolithography®: a “Desktop Nanofab™” approach using high-throughput flexible nanopatterning. Scanning 2008;30:137–50.
[54] Dobrik G, Tapasztó L, Nemes-Incze P, Lambin Ph, Biró LP. Crystallographically oriented high resolution lithography of graphene nanoribbons by STM lithography. Phys State Solidi A 2010;247:896–902.
[55] Hahn JR, Kang H, Song S, Jeon IC. Observation of charge enhancement induced by graphite atomic vacancy: a comparative STM and AFM study. Phys Rev B 1996;53:R1725–8.
[56] Hölscher H, Allers W, Schwarz UD, Schwarz A, Wiesendanger R. Interpretation of “true atomic resolution” images of graphite (0 0 0 1) in noncontact atomic force microscopy. Phys Rev B 2000;62:6967–70.
[57] Kim D-H, Koo J-Y, Kim J-J. Cutting of multiwalled carbon nanotubes by a negative voltage tip of an atomic force microscope: a possible mechanism. Phys Rev B 2003;68:113406-1–4.
[58] Park JG, Zhang C, Liang R, Wang B. Nano-machining of highly oriented pyrolytic graphite using conductive atomic force microscope tips and carbon nanotubes. Nanotechnology 2007;18:405306–12.
[59] Weng L, Zhang L, Chen YP, Rokhinson LP. Atomic force microscope local oxidation nanolithography of graphene. Appl Phys Lett 2008;93:093107-1–3.

[60] Nemes-Incze P, Osváth Z, Kamarás K, Biró LP. Anomalies in thickness measurements of graphene and few layer graphite crystals by tapping mode atomic force microscopy. Carbon 2008;46:1435–42.
[61] Giesbers AJM, Zeitler U, Neubeck S, Freitag FF, Novoselov KS, Maan JC. Nanolithography and manipulation of graphene using an atomic force microscope. Solid State Commun 2008;147:366–9.
[62] Campos LC, Manfrinato VR, Sanchez-Yamagishi JD, Kong J, Jarillo-Herrero P. Anisotropic etching and nanoribbon formation in single-layer graphene. Nano Lett 2009;9(7):2600–4.
[63] Datta SS, Strachan DR, Khamis SM, Johnson ATC. Crystallographic etching of few-layer graphene. Nano Lett 2008;8:1912–5.
[64] Konishi S, Sugimoto W, Murakami Y, Takasu Y. Catalytic creation of channels in the surface layers of highly oriented pyrolytic graphite by cobalt nanoparticles. Carbon 2006;44:2330–56.
[65] Schäffel F, Warner JH, Bachmatiuk A, Rellinghaus B, Büchner B, Schultz L, et al. Shedding light on the crystallographic etching of multi-layer graphene at the atomic scale. Nano Res 2009;2:695–705.
[66] Severin N, Kirstein S, Sokolov IM, Rabe JP. Rapid trench channeling of graphenes with catalytic silver nanoparticles JP. Nano Lett 2009;9(1):457–61.
[67] Gao L, Ren W, Liu B, Wu Z-S, Jiang C, Cheng H-M. Crystallographic tailoring of graphene by nonmetal SiO_x nanoparticles. J Am Chem Soc 2009;131:13934–6.
[68] Fonseca A, Hernadi K, Piedigrosso P, Colomer JF, Mukhopadhyay K, Doome R, et al. Synthesis of single- and multi-wall carbon nanotubes over supported catalysts. Appl Phys A 1998;67:11–22.
[69] McKee DW. Effect of metallic impurities on the gasification of graphite in water vapor and hydrogen. Carbon 1974;12:453–64.
[70] Harris PS, Feates FS, Reuben BG. Controlled atmosphere electron microscopy studies of graphite gasification—4. Catalysis of the graphite–O_2 reaction by silver. Carbon 1974;12:189–97.
[71] Koh SJ. Controlled placement of nanoscale building blocks: toward large-scale fabrication of nanoscale devices. JOM J Miner, Met Mater Soc 2007;59:22–8.
[72] Ma L-C, Subramanian R, Huang H-W, Ray V, Kim C-U, Koh SJ. Electrostatic funneling for precise nanoparticle placement: a route to wafer-scale integration. Nano Lett 2007;7:439–45.
[73] Radovic LR, Bockrath B. On the chemical nature of graphene edges: origin of stability and potential for magnetism in carbon materials. J Am Chem Soc 2005;127:5917–27.
[74] Jiang D-E, Sumpter BG, Dai S. Unique chemical reactivity of a graphene nanoribbon's zigzag edge. J Chem Phys 2007;126:134701-1–6.
[75] Osváth Z, Darabont A, Nemes-Incze P, Horváth E, Horváth ZE, Biró LP. Graphene layers from thermal oxidation of exfoliated graphite plates. Carbon 2007;45:3022–6.
[76] Byon HR, Choi HC. Carbon nanotube guided formation of silicon oxide nanotrenches. Nat Nanotechnol 2007;2:162–6.
[77] Nemes-Incze P, Magda G, Kamarás K, Biró LP. Crystallographically selective nanopatterning of graphene on SiO_2. Nano Res 2010;3:110–6.
[78] Koskinen P, Malola S, Hakkinen H. Self-passivating edge reconstructions of graphene. Phys Rev Lett 2008;101:115502-1–4.
[79] Jia X, Hofmann M, Meunier V, Sumpter BG, Campos-Delgado J, Romo-Herrera JM, et al. Controlled formation of sharp zigzag and armchair edges in graphitic nanoribbons. Science 2009;323:1701–5.
[80] Girit CÖ, Meyer JC, Erni R, Rossell MD, Kisielowski C, Yang L, et al. Graphene at the edge: stability and dynamics. Science 2009;323:1705–8.
[81] Koskinen P, Malola S, Hakkinen H. Evidence for graphene edges beyond zigzag and armchair. Phys Rev B 2009;80:073401-1–3.
[82] Liu Z, Suenaga K, Harris PJF, Iijima S. Open and closed edges of graphene layers. Phys Rev Lett 2009;102:015501-1–4.